Mass spectrometry imaging for *in situ* kinetic histochemistry

Katherine B. Louie[1§], Benjamin P. Bowen[1§], Stephanie McAlhany[3], Yurong Huang[1], John C. Price[4], Jian-hua Mao[1], Marc Hellerstein[2,3,4] and Trent R. Northen[1*]

SUPPLEMENTARY TABLES AND FIGURES

Serum Deuterium Enrichment

Sample	Average Atom % D
Serum, deuterium-enriched mouse	4.50
Serum, control mouse	0.0149

Supplementary Table S1. Measurement of atom% D in body water. To rapidly achieve a stable concentration of ^2H_2O in body water, a concentrated bolus dose of ^2H_2O followed by 8% ^2H_2O in drinking water was administered to a tumor-bearing mouse[1]. After 5 days, this resulted in final body water enrichment of 4.5 atom% ^2H, as measured using cavity ringdown spectroscopy. This value is comparable to previous studies for the given dosage of ^2H_2O in drinking water[2]. Since body water serves as the precursor pool of deuterated water used in active metabolism, atom% ^2H provides a measure of the fractional amount of hydrogen atoms on a molecule capable of being metabolically replaced with ^2H[3].

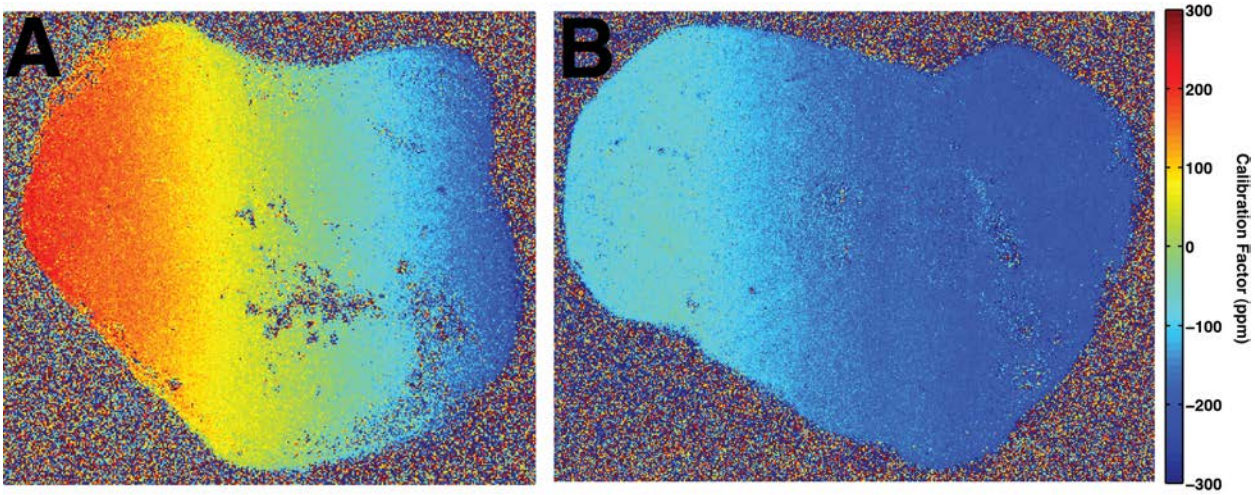

Supplementary Figure S1. These images plot the calibration factor implemented for each pixel in the (**A**) control, unlabeled tumor and (**B**) deuterium-enriched tumor. The calibration factor is calculated as the required shift in each measured spectrum that minimizes the distance between the measured and reference masses.

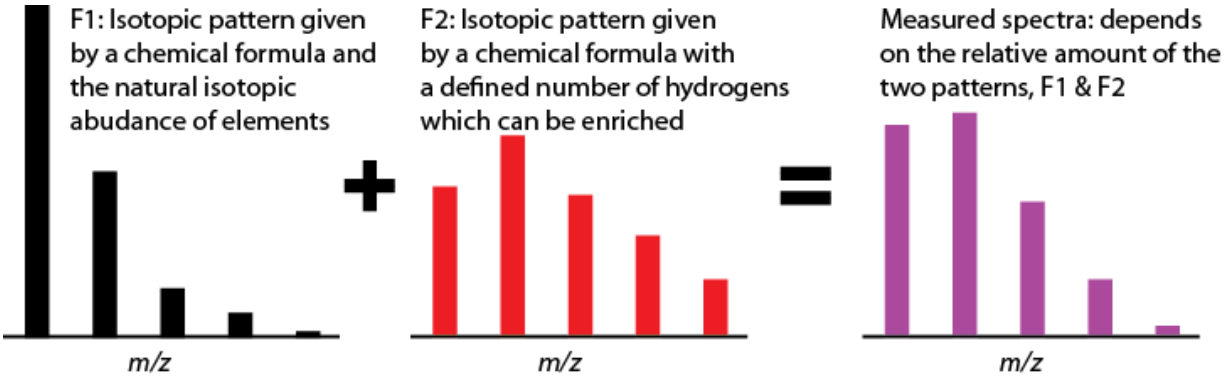

Supplementary Figure S2. For each of the 45 lipid species considered in this study, two patterns are required to model the observed data: (1) the natural isotopic pattern for each compound, $F1_i$ and (2) the enriched isotopic pattern for each compound, $F2_i$. The linear coefficients of these 90 patterns (2 for each lipid species – ^{2}H-labeled vs. unlabeled) and an offset term were solved by least-squares fitting in which the coefficients were subject to non-negativity constraints for each pixel.

Validation of values for *N*. To evaluate selected values of *N* for each lipid, the isotopic enrichment model was also implemented using alternate values of *N*. Quality of fit over a range of values was tested by shifting or scaling the values of *N* (**Supplementary Fig. S3**) by +/- 50% or +/-15, respectively. Spectra with pixels having total intensity in the top 5th percentile were modeled by non-negative least squares fitting of the isotopic enrichment model. Plots in Supplementary Fig. S3 show the average error minima is within only 5% or 2 hydrogen atoms from our selected values for *N*.

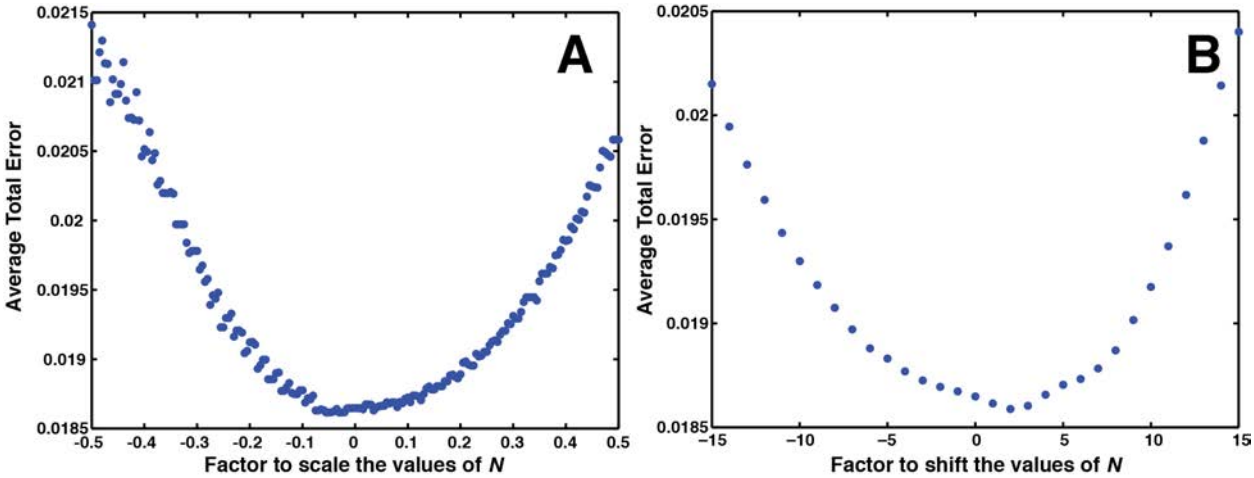

Supplementary Figure S3. Calculation of error using alternate values of *N*, the maximum number of hydrogen sites originating from water. In panel **A**, alternative values of *N* are calculated by scaling the original values by a factor (+/- 50%). Modifying *N* by approximately +/- 10% has little effect on the overall quality of the fit. In panel **B**, new values of *N* are calculated by directly adding or subtracting +/- 15 hydrogens to each value of *N* in the model. Modifying *N* by approximately +/- 5 has little effect on the overall quality of the fit.

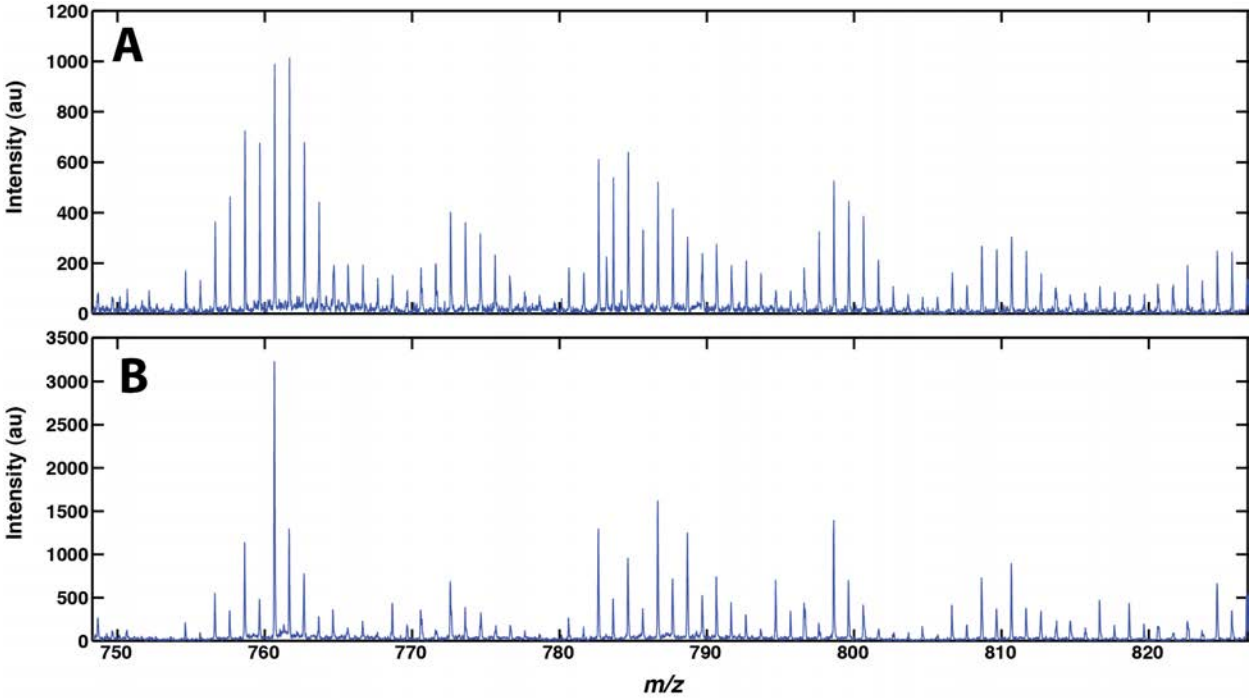

Supplementary Figure S4. Mass spectra generated from extracts spotted directly onto a NIMS chip from a (**A**) labeled and (**B**) unlabeled tumor. By visual inspection, the frequency in which the M1 isotopologue's intensity is either greater or near to the M0 isotopologue's (monoisotopic mass) intensity indicates deuterium enrichment in the labeled tumor and not in the unlabeled.

Identified lipid species detected in tumor

#	Compound ID	Monoisotopic mass		Chemical Formula	*N*	Normalized Abundance (0-1)	Mass error (ppm)		Fragments (MS/MS, PSD)
		$[M+H]^+$	$[M+K]^+$				NIMS, tumor tissue	LC/MS, tumor extract	
1-a	PC(34:05)	752.5225	790.4784	C42H74NO8P	30	0.052	**3.5**	**3.4**	184
1-b	PE(P-38:04)	752.5589	790.5148	C43H78NO7P	39	0.022	49.6	**0.1**	
2-a	PC(34:04)	754.5381	792.4940	C42H76NO8P	33	0.042	**4.8**	**4.4**	184
3-a	PC(34:03)	756.5538	794.5097	C42H78NO8P	36	0.175	**2.7**	**0.5**	184
4-a	PC(34:02)	758.5694	796.5253	C42H80NO8P	39	1.000	**2.4**	**2.3**	184
4-b	PS(34:03)	758.4967	796.4526	C40H72NO10P	35	0.018	1174.5	14.8	
5-a	PC(34:01)	760.5851	798.5410	C42H82NO8P	42	0.894	26.9	**1.9**	184
5-b	PS(34:02)	760.5123	798.4682	C40H74NO10P	39	0.018	64.2	**2.6**	
6-a	PC(34:00)	762.6007	800.5566	C42H84NO8P	45	0.026	72.0	**0.6**	184
6-b	PS(34:01)	762.5280	800.4839	C40H76NO10P	42	0.026	18.9	**0.7**	
7-b	PE(38:06)	764.5225	802.4784	C43H74NO8P	33	0.017	41.0	10.2	
7-a	PS(34:00)	764.5436	802.4995	C40H78NO10P	45	0.009	14.7	**1.1**	
8-a	PE(38:05)	766.5381	804.4940	C43H76NO8P	36	0.079	39.8	**0.4**	-141(NL)
8-b	PC(P-36:04)	766.5745	804.5304	C44H80NO7P	36	0.046	5.4	5.6	184
9-b	PE(38:04)	768.5538	806.5097	C43H78NO8P	39	0.083	41.8	**0.5**	-141(NL)
9-a	PC(P-36:03)	768.5902	806.5461	C44H82NO7P	39	0.080	**3.3**	**1.6**	184
10-a	PC(P-36:02)	770.6058	808.5617	C44H84NO7P	42	0.010	16.9	45.5	184
11-a	PE(38:02)	772.5851	810.5410	C43H82NO8P	45	0.021	**1.2**	**1.0**	
11-b	PC(P-36:01)	772.6215	810.5774	C44H86NO7P	45	0.014	46.1	6.4	184
12-a	PE(P-40:07)	774.5432	812.4991	C47H80NO7P	33	0.052	62.1	7.9	
12-b	PE(38:01)	774.6007	812.5566	C43H84NO8P	48	0.010	8.7	7.5	
13-a	PE(P-40:06)	776.5589	814.5148	C47H82NO7P	36	0.007	20.1	19.7	
14-a	PC(36:06)	778.5381	816.4940	C44H76NO8P	30	0.017	7.2	**4.3**	
15-a	PC(36:05)	780.5538	818.5097	C44H78NO8P	33	0.143	9.9	**0.2**	184
16-a	PC(36:04)	782.5694	820.5253	C44H80NO8P	36	0.798	5.2	**1.9**	184
17-a	PC(36:03)	784.5751	822.5310	C44H82NO8P	39	0.436	14.6	14.9	184
17-b	PS(36:04)	784.5123	822.4682	C42H74NO10P	36	0.014	90.9	**0.9**	
18-a	PC(36:02)	786.6007	824.5566	C44H84NO8P	42	0.265	24.2	**2.8**	184
18-b	PS(36:03)	786.5280	824.4839	C42H76NO10P	39	0.013	64.1	**4.7**	
19-a	PS(36:02)	788.5436	826.4995	C42H78NO10P	42	0.094	21.7	**2.0**	
19-b	PC(36:01)	788.6164	826.5723	C44H86NO8P	45	0.069	66.3	**2.4**	184
20-a	PS(36:01)	790.5593	828.5152	C42H80NO10P	45	0.076	19.6	**0.7**	
21-a	PC(P-38:05)	792.5902	830.5461	C46H82NO7P	36	0.050	**2.1**	**0.6**	184
21-b	PS(36:00)	792.5749	830.5308	C42H82NO10P	48	0.015	20.4	**0.3**	
22-a	PC(P-38:04)	794.6058	832.5617	C46H84NO7P	39	0.124	12.6	**0.1**	184
23-a	PE(40:04)	796.5851	834.5410	C45H82NO8P	42	0.017	**0.7**	**3.8**	
23-b	PC(P-38:03)	796.6215	834.5774	C46H86NO7P	42	0.014	42.9	**1.2**	184
24-a	PC(P-38:02)	798.6371	836.5930	C46H88NO7P	45	0.002	51.7	10.4	184
25-a	PE(40:02)	800.6164	838.5723	C45H86NO8P	48	0.003	32.6	**2.8**	
26-a	PC(38:08)	802.5381	840.4940	C46H76NO8P	27	0.037	**2.3**	**4.6**	184
27-a	PC(38:07)	804.5538	842.5097	C46H78NO8P	30	0.022	**2.0**	**2.6**	184
28-a	PC(38:06)	806.5694	844.5253	C46H80NO8P	33	0.120	**4.5**	**1.4**	184
29-a	PC(38:05)	808.5851	846.5410	C46H82NO8P	36	0.279	8.5	**0.6**	184
30-a	PC(38:04)	810.6007	848.5566	C46H84NO8P	39	0.260	18.7	**1.1**	184
30.5-b	SM(d42:03)	811.6688	849.6247	C47H91N2O6P	53	0.025	84.5	15.5	
31-a	PS(38:04)	812.5436	850.4995	C44H78NO10P	39	0.158	41.2	**0.8**	
31-b	PE(P-42:02)	812.6528	850.6087	C47H90NO7P	53	0.107	87.1	**1.0**	
31.5-b	SM(d42:02)	813.6844	851.6403	C47H93N2O6P	56	0.042	126.8	**2.8**	
32-a	PS(38:03)	814.5593	852.5152	C44H80NO10P	42	0.028	18.2	**1.8**	
32.5-b	SM(d42:01)	815.7001	853.6560	C47H95N2O6P	59	0.008	129.6	**1.0**	
33-a	PC(P-40:07)	816.5902	854.5461	C48H82NO7P	33	0.014	**1.5**	**3.1**	184
34-a	PC(P-40:06)	818.6058	856.5617	C48H84NO7P	36	0.028	**0.5**	**0.4**	184
35-a	PC(P-40:05)	820.6215	858.5774	C48H86NO7P	39	0.008	15.0	13.3	184
36-a	PC(P-40:04)	822.6371	860.5930	C48H88NO7P	42	0.007	63.1	**4.3**	184
37-a	PC(P-40:03)	824.6528	862.6087	C48H90NO7P	45	0.004	108.4	19.1	
38-a	PC(40:10)	826.5381	864.4940	C48H76NO8P	24	0.003	**0.2**	34.2	
39-a	PC(40:09)	828.5538	866.5097	C48H78NO8P	27	0.007	**3.9**	11.5	184
40-a	PC(40:08)	830.5694	868.5253	C48H80NO8P	30	0.139	**4.8**	**0.2**	
41-a	PC(40:07)	832.5851	870.5410	C48H82NO8P	33	0.038	**3.2**	**0.3**	
42-a	PC(40:06)	834.5983	872.5542	C48H84NO8P	36	0.025	**4.0**	**0.1**	
43-a	PS(40:06)	836.5436	874.4995	C46H78NO10P	36	0.063	73.4	**0.6**	
43-b	PC(40:05)	836.6091	874.5650	C48H86NO8P	39	0.023	**1.5**	7.2	
44-a	PS(40:05)	838.5593	876.5152	C46H80NO10P	39	0.021	28.8	**1.0**	
44-b	PC(40:04)	838.6320	876.5879	C48H88NO8P	42	0.008	54.2	**0.9**	
45-a	PS(40:04)	840.5749	878.5308	C46H82NO10P	42	0.026	**4.9**	**0.5**	

Supplementary Table S2. Identified phospholipid compounds in tumor mass spectra. The monoisotopic mass of each identified compound is shown for both $[M+H]^+$ and $[M+K]^+$ adducts. The mass error, or difference between measured mass and monoisotopic mass (ppm), is shown for mass spectra from direct NIMS imaging (comparing $[M+K]^+$ adducts) of tumor tissue and LC/MS (comparing $[M+H]^+$ adducts) of tumor extract Values <30ppm are shaded, with values <5ppm in bold. The last column shows detection of the characteristic fragment ions (m/z = 184 for PC, neutral loss of -141 for PE) using LC/MS/MS or post source decay (PSD). Values of *N* used in the model of isotopic enrichment are also shown. The relative levels of each lipid in the tumor extract are also shown.

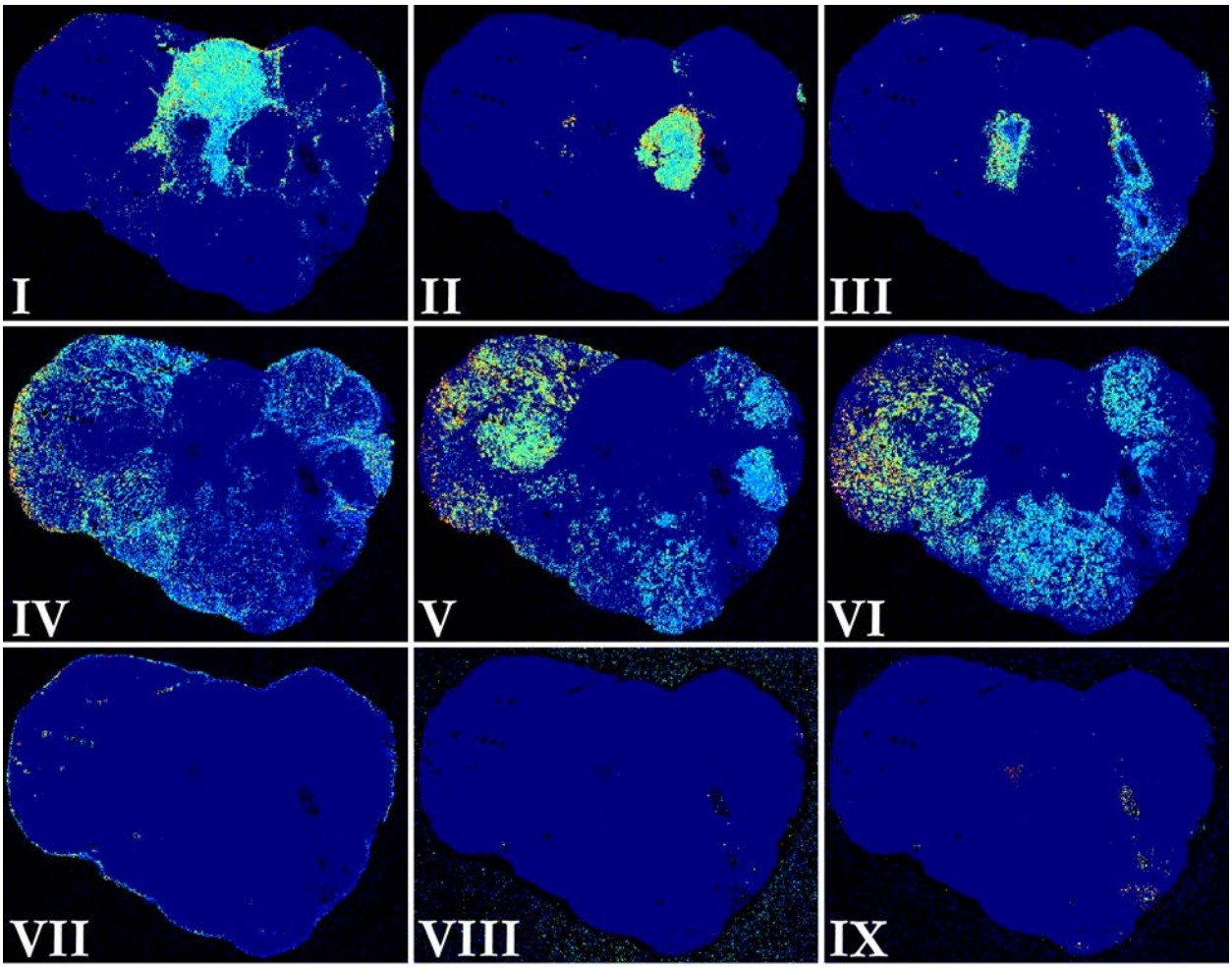

Supplementary Figure S5. Images of the nine regions identified in the deuterium-enriched tumor by applying K-means analysis. This approach identified 3 regions associated with background (Regions VII-IX) and 6 regions associated with the tumor (Regions I-VI).

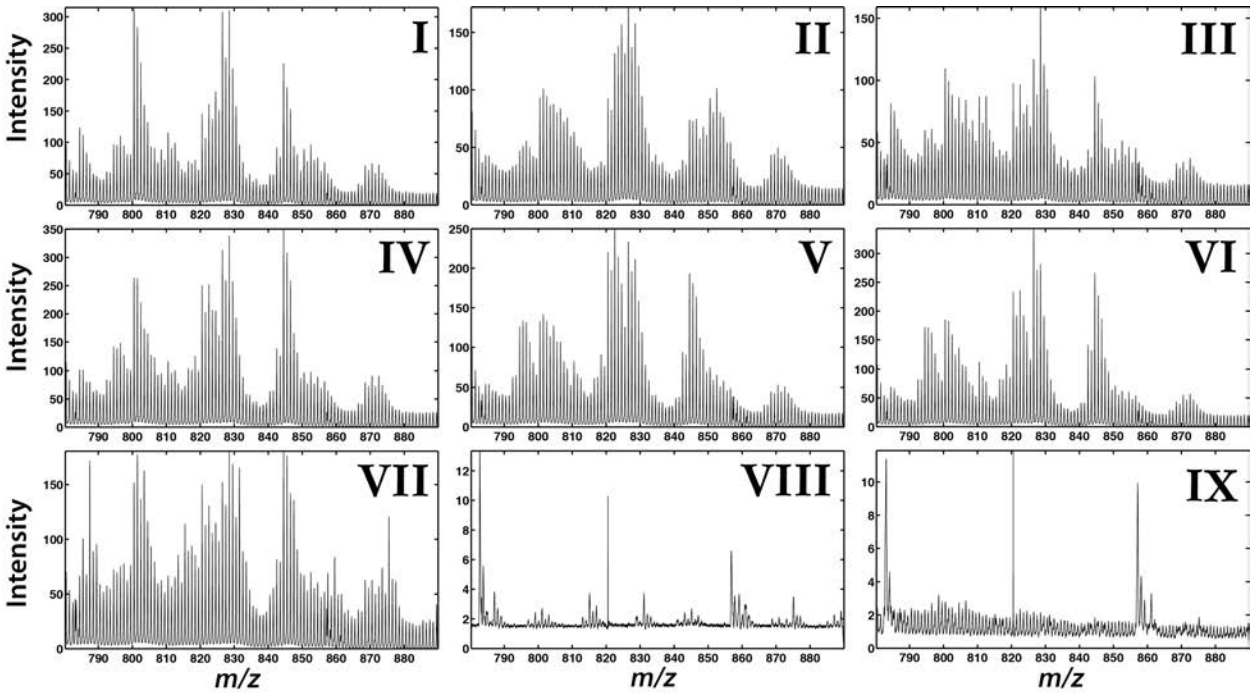

Supplementary Figure S6. Average spectra corresponding to the nine regions identified in the deuterium-enriched tumor by applying K-means analysis.

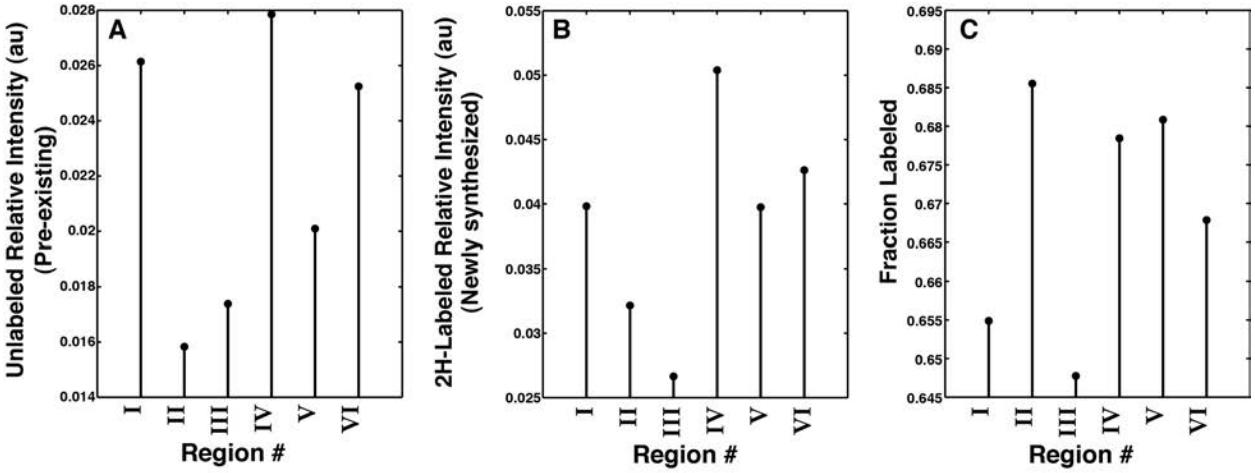

Supplementary Figure S7. To compare relative levels of new synthesis and turnover between K-means regions, the normalized, average intensity originating from (**A**) unlabeled and (**B**) ^{2}H-labeled lipids is shown for Regions I-VI. Panel (**C**) plots the *fraction* of total signal originating from newly synthesized (labeled) lipids for each region. Region II, characterized as having high grade features of malignancy according to H&E, has the lowest levels of pre-existing lipids (**Panel A**) and the highest fraction of newly synthesized lipids (**Panel C**). Region III, characterized as necrotic according to H&E, has the lowest levels of newly synthesized lipids overall (**Panel B**).

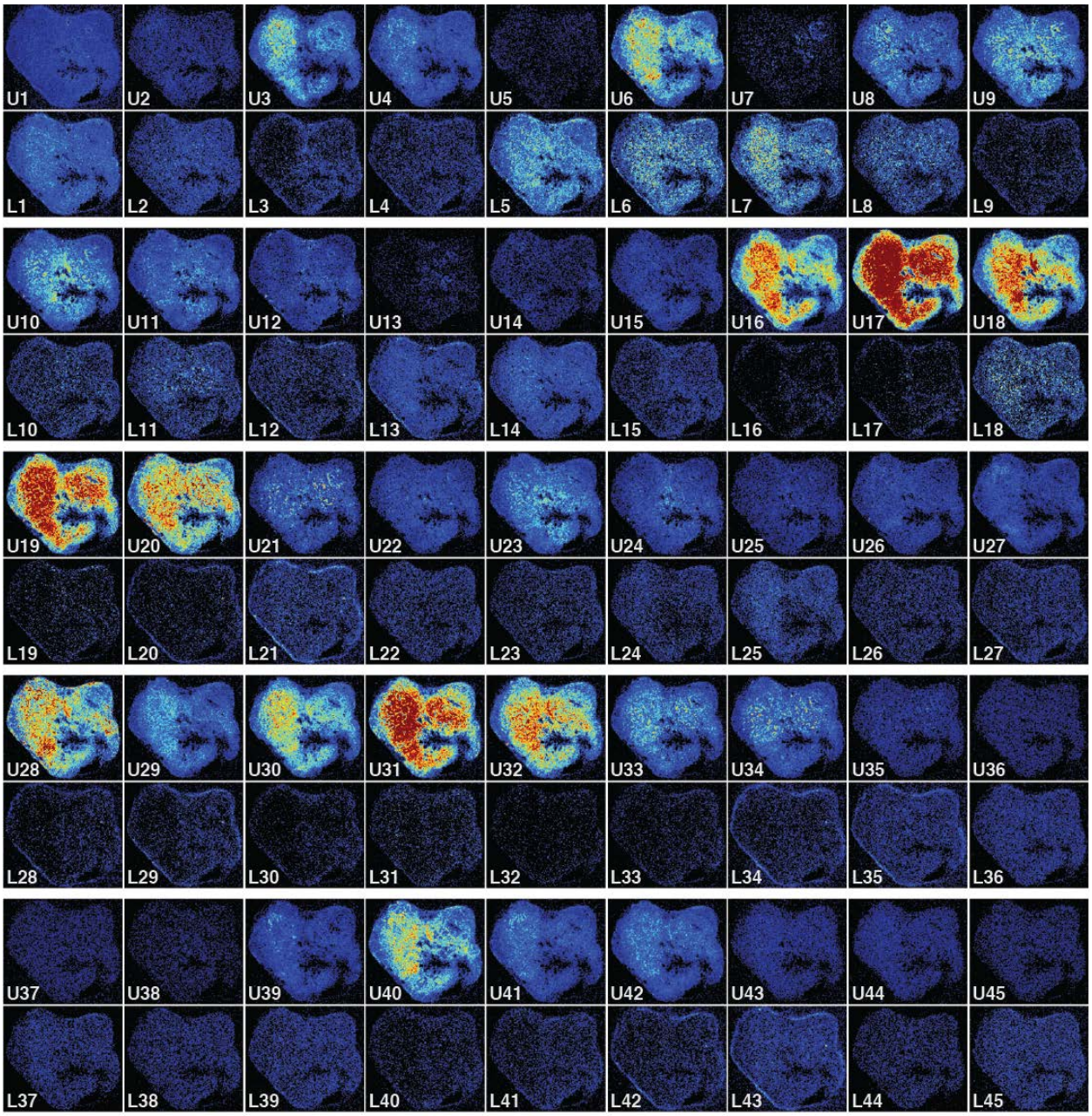

Supplementary Figure S8. Intensity images of the **unlabeled, control tumor** for the 45 phospholipids identified in this study, where each column represents a unique lipid. For each block, the top row is unlabeled (pre-existing) and bottom row is ^{2}H-labeled (newly synthesized). The false color scale indicates the relative level of each lipid, maximally labeled or unlabeled, distributed throughout the tissue. Image subscripts link to Supplementary Table 2 corresponding to specific lipid species. U=unlabeled, L= labeled, F=fraction labeled.

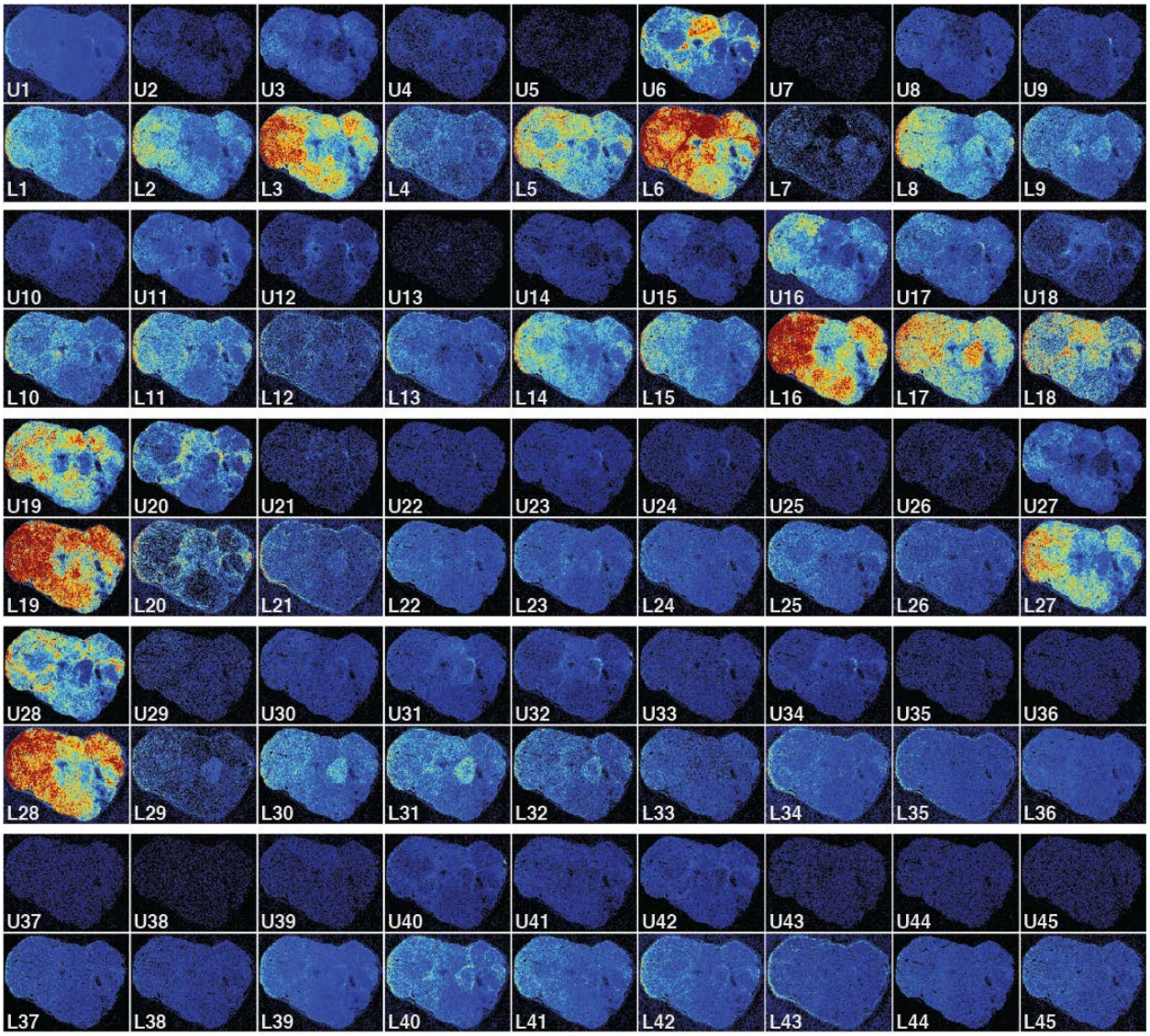

Supplementary Figure S9. Intensity images of the **deuterium-enriched tumor** for the 45 phospholipids identified in this study, where each column represents a unique lipid. For each block, the top row is unlabeled (pre-existing) and bottom row is ^{2}H-labeled (newly synthesized). The false color scale indicates the relative level of each lipid, maximally labeled or unlabeled, distributed throughout the tissue. Image subscripts link to Supplementary Table 2 corresponding to specific lipid species. U=unlabeled, L= labeled, F=fraction labeled.

Histopathology findings. Results from the blinded histopathology examination of the H&E stain of the deuterium-enriched tumor.

All tissue represents tumor with no normal appearing breast parenchyma. Below are three figures with specific findings associated with each figure.

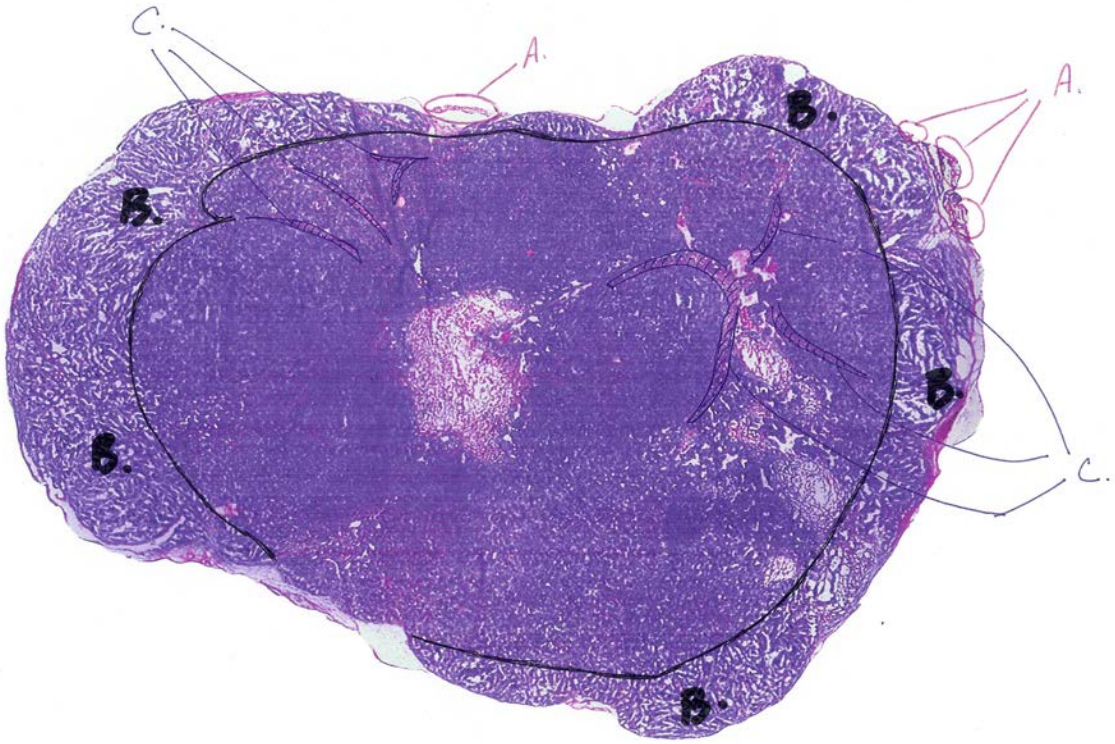

Supplementary Figure S10. A (red). Small peripheral areas of adherent skeletal muscle are noted, as marked. **B (black).** All of tissue has moderate frozen section artifact, more pronounced artifact peripherally, as marked. **C (blue).** All of tissue has delicate intersecting fibrous tissue. Larger fibrous septa are as marked. Sheet #1.

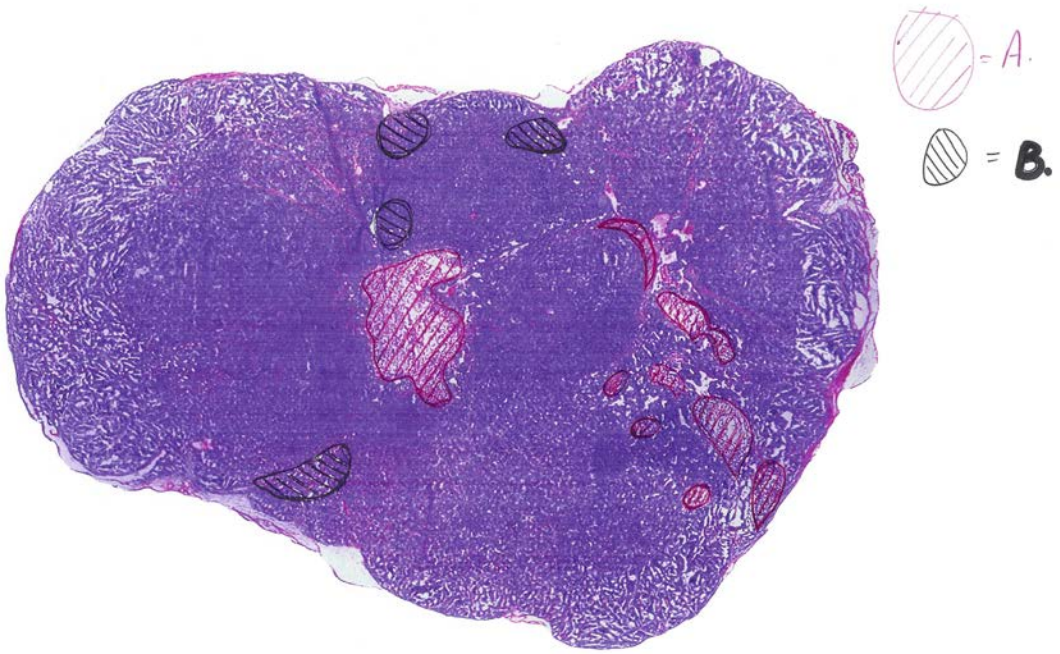

Supplementary Figure S11. A (red). Variable sized zones of tumor necrosis (with apoptotic bodies and cell ghosts) are present. **B (black).** Architecture is variable with most areas showing *very* poorly-formed glandular structures along the delicate intersecting fibrous tissue. Areas with *slightly* better formed glandular structures are as marked. Sheet #2.

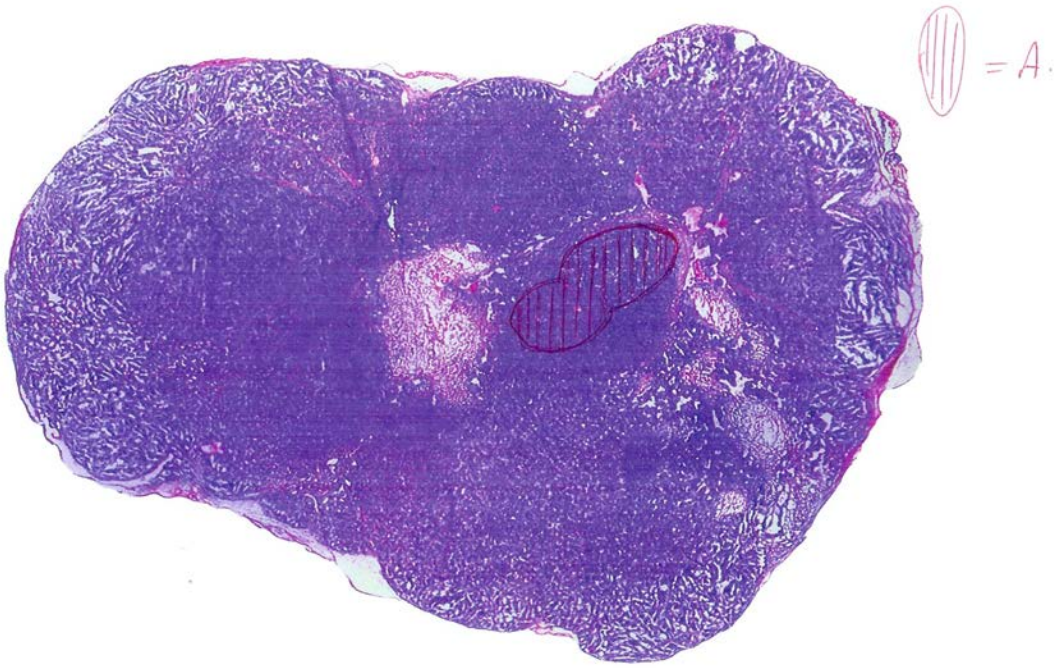

Supplementary Figure S12. A(red). Most of the tumor is composed of intermediate to large sized cells with moderate pleomorphism. One area shows marked pleomorphism with "bizarre" nuclei and cells with multiple nuclei. Sheet #3.

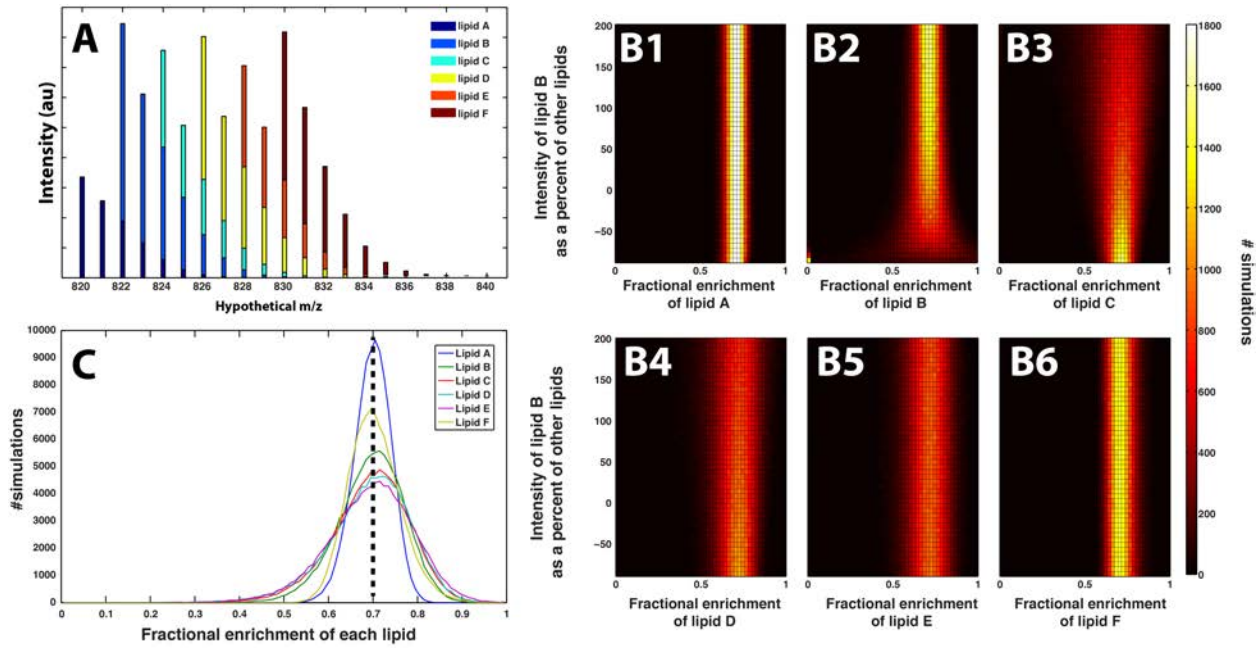

Supplementary Figure S13. Sensitivity analysis to examine the influence of relative abundance of a particular lipid species on calculated isotopic enrichment of other lipids. Six hypothetical lipids (denoted A-F) were considered for this simulation. **(Panel A)** Contribution of each lipid to the total spectrum. **(Panels B and C)** Lipid B's relative abundance (intensity) was varied while all other lipids were held constant. All lipids were held at a constant fractional enrichment (0.7) and the intensity of lipid B was varied from near zero to 200% (y-axis). In Panel B, the average fractional enrichment (x-axis) remains centered at 0.7. In Panel C, integration of each lipid over all intensities of B results in Gaussian distributions also centered at 0.7. [Simulation details: Each fit was performed 10,000 times with the addition of a random amount of noise. The noise added or subtracted to each peak was from a random number generated from a Gaussian distribution, and a generous amount (5%) of noise was used for these simulations. The hypothetic lipids were simulated as diacyl phosphocholine lipids differing in their degree of saturation.]

Supplementary References

1. Turner, S.M. et al. Measurement of TG synthesis and turnover in vivo by 2H2O incorporation into the glycerol moiety and application of MIDA. *American journal of physiology. Endocrinology and metabolism* **285**, E790-803 (2003).
2. Lee, W.N.P. et al. In-Vivo Measurement of Fatty-Acids and Cholesterol-Synthesis Using D2o and Mass Isotopomer Analysis. *Am J Physiol* **266**, E699-E708 (1994).
3. Diraison, F., Pachiaudi, C. & Beylot, M. In vivo measurement of plasma cholesterol and fatty acid synthesis with deuterated water: determination of the average number of deuterium atoms incorporated. *Metabolism: clinical and experimental* **45**, 817-821 (1996).